Fundamental Issues and Applications of
Shock-Wave and High-Strain-Rate Phenomena
K.P. Staudhammer, L.E. Murr, and M.A. Meyers (Editors)

Chapter 27

Dynamic behavior of silicon carbide

C.J. Shih, M.A. Meyers, and V.F. Nesterenko

Department of Mechanical and Aerospace Engineering, University of California, San Diego La Jolla, CA 92093

Silicon carbide was subjected to dynamic deformation in (a) a compression Hopkinson-Kolsky bar (compressive stresses of 5 GPa), and (b) high-velocity impact under confinement (compressive stresses of 19 GPa) by a cylindrical tungsten alloy projectile, and (c) in the radial collapse of pre-fragmented or granular ceramic in a thick-walled cylinder geometry. Shear localization was observed to accommodate the large permanent deformation in the radial collapse geometry. Localization occurred by two different micromechanical modes: for larger fragments, the material within the shear bands was finely pulverized; for smaller particles, the material within the shear zones exhibited the effects of heating and subsequent sintering. For specimens from the Hopkinson bar and confined impact experiments, considerable evidence of plastic deformation, as dislocations and stacking faults, was observed in the recovered fragments. Profuse dislocation activity was observed in the frontal layer in the specimen recovered from the projectile impact. The formation of this layer is enabled by the high lateral confinement. Plastic deformation is consistent with an analysis based on the competition between crack growth under compression and dislocation generation. Different mechanisms are discussed for the initiation of fracture; (a) dilatant cracks induced by mismatch in the effective elastic moduli between two adjacent grains, leading to internal tensile stresses and creating transgranular fracture; (b) Zener-Stroh cracks nucleated by the piled up dislocations along grain boundaries, and resulting in intergranular fracture ; (c) cracks due to existing flaws; (d) stress concentrations due to twinning and stacking faults. Heat transfer calculations are carried out that show: (a) the intact layer between the Mescall zone and the impact interface is not due to heating and sintering, but due to unique state of confinement provided by the uniaxial strain state, and (b) that the temperatures within the shear zones can reach values of 2,500 K, consistent with the observation of sintering.

1. INTRODUCTION

Ceramics possess the high hardness, toughness, and low density that render them unique as armor materials [1]. Among ceramics, silicon carbide has been the object of substantial studies. The four basic material's phenomena that occur when a projectile hits an armor are: (a) propagation of shock stress wave; (b) radial cracking; (c) comminution and ejection of comminuted material; (d) reflection of stress wave within armor system. In an effort to elucidate the fundamental mechanisms occurring during armor penetration, experiments were coupled with analysis and characterization of SiC. Three types of experiments were carried out: (a) unconfined dynamic compression tests; (b) impact under confined condition (interface defeat setup); (c) collapse of a thick-walled cylinder composed of damaged or granular ceramic. The detailed results of this investigation appear somewhere else [2-4].

2. EXPERIMENTAL MATERIALS AND METHODS

Two different solid silicon carbides (designated by SiC-I and SiC-II) were investigated in this study. Standard hot pressing procedures were used to fabricate these materials where α-SiC powder was first mixed with sintering aids. The blended powder was loaded into a graphite die and then hot pressed above 2000°C at 18 MPa under a controlled atmosphere. SiC-I is a conventional SiC, using boron and carbon as sintering aids. The carbon removes the oxide layer which inhibits the densification. SiC-II, using an Al-based compound as the sintering aid, is a ballistic grade SiC, commercially sold as CERCOM SiC-B. Silicon carbide powders with three different particle sizes

were also used in this investigation. The average particle sizes for the small, medium and coarse powders were 0.4, 3 and 50 μm, respectively.

In order to accurately investigate the deformation of ceramics, the following modifications were applied to the Hopkinson bars: (1) *a pulse shaper,* placed in front of the incident bar to ensure uniform stress, (2) *a momentum trap*, to allow the specimen to undergo single loading, (3) *a strain gage* on the specimen to accurately measure the strain in the specimen, and (4) a pair of *contact platens* sandwiching the ceramic specimen to prevent damage in the steel bars while the specimen was catastrophically fractured. SiC whisker-reinforced Si_3N_4 composite was selected for the contact platens, because of its high strength (900 MPa flexural strength) and fracture toughness (8 MPa). This elastic pulse deforms the SiC specimen in a uniaxial stress condition in the absence of lateral confinement. SiC was dynamically stressed using the modified split Kolsky-Hopkinson bar at a strain rate between 400 and 800 s^{-1}.

In real armor applications, material inertia imposes a lateral confinement, and the strain rate is higher than the strain rate achieved in the split Hopkinson-Kolsky bar test. Hauver et al. [5-7] developed a testing method to defeat the long rod projectile at a high velocity (1.5 km/s), in front of the ceramic target. A shock-wave attenuator was placed in front of the ceramic target to reduce the shock-wave damage in the ceramic. The ceramic was confined through a shrink-fit metal casing, and the confinement pressure was a few hundred MPa. Interface coupling was applied on the ceramic front face to allow the plastic deformation and flow of the penetrator. This type of testing configuration allowed the recovery of the impacted specimens for further microstructural characterization.

The thick-walled cylinder method was used to investigate the high-strain-rate deformation (3 x 10^4 s^{-1}) of prefractured and granular silicon carbide. The experimental procedures were originally developed for metals and were later modified for granular and brittle materials[8-10]. The monolithic silicon carbide was prefractured by passing a shock wave through the assembly[11]. Experiments were conducted on fine, medium, and coarse powder specimens(0.4, 3, and 50 μm), which were tested under identical conditions. The procedure consists of two explosive events: the first event to densify (or to fragment monolithic ceramic) the ceramic and the second event to deform the densified/ prefractured ceramic.

The experimental procedures are outlined in Figure 1. Silicon carbide powder was loaded into a tubular cavity made up by a central copper rod and an outer copper tube. A mixture of 3 : 1 volume ratio of ammonite and sand was used to generate an explosion of low detonation velocity to densify/fragment the SiC cylinder.

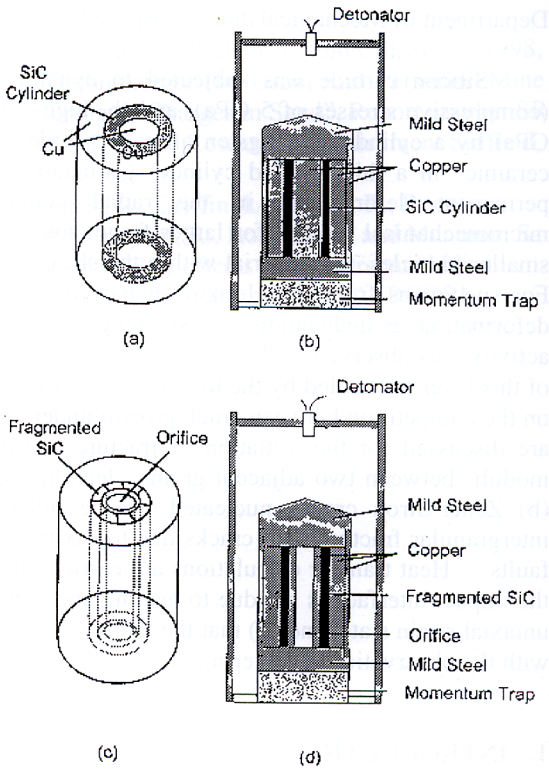

Figure 1. Experimental procedures: (a) specimen assembly, (b) first explosive event: fragmentation of solid or densification of granular ceramic, (c) orifice drilling, and (d) second explosive event: deformation of fragmented/densified ceramic.

A cylindrical orifice was then drilled in the center of the copper insert. The specimen then underwent another explosive event. This explosive event produced large inelastic deformation and profuse shear bands. The global strains can be obtained from the strains in the incompressible copper; i.e., the cross-sectional area of copper along the longitudinal axis remains the same during deformation. The radial and tangential engineering strains (ε_{rr} and $\varepsilon_{\varphi\varphi}$) and effective strain ($\varepsilon_{eff}$) can be

estimated from the initial and final radii, r_o and r_f. The strain rate during the test is calculated from the measured displacement of the inner wall of the cylinder during the collapse process , and the strain rate is approximately 3×10^4 s^{-1}.

3. DYNAMIC COMPRESSION STRENGTH

Lankford [12,13] showed first that ceramics (including SiC) exhibited a strain rate dependence of compressive strength. The current results are shown, together with Lankford's results, in Figure 2. The average compressive strengths of SiC-I and SiC-II are 4.7 and 5.1 GPa, respectively.

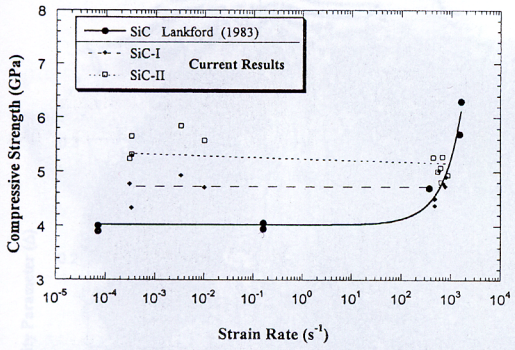

Figure 2. Compressive strength of SiC as a function of strain rate.

The average quasistatic compressive strengths of SiC-I and SiC-II were 4.8 and 5.4 GPa, respectively. These values are significantly higher than Lankford's data (4.0 GPa). Great care was taken in specimen preparation, both for quasistatic and dynamic tests. Specimens were polished to a mirror finish, and the parallelism of the compressive surfaces was controlled to within 5 μm. It was found that the alignment of the loading is crucial in compressive testing and that polishing of the specimens had little effect. During quasistatic testing, in addition to the self-aligned compressive fixture, two steel foils (25 μm thick) were placed on the compressive surfaces to ensure the alignment of the applied force. As shown in Figure 2, the strain rate effect, reported by Lankford [12,13], activates when the strain rates are higher than 10^3 s^{-1}; the current testing configuration could only achieve strain rates up to 800 s^{-1}. In our modified split Hopkinson bar testing, a pulse shaper was placed in front of the incident bar to ensure a uniform stress. The plastic deformation of the pulse shaper increased the rise time during loading, but also reduced the strain rate of the ceramic specimen. The increase in compressive strength of ceramics, at strain rates on the order of 10^3 s^{-1} and higher, has been analytically predicted by Ravichandran and Subhash [14]. They proposed an expression for the critical strain rate at which the strength becomes significantly strain-rate dependent. From elasticity

$$\dot{\varepsilon}^* = \frac{\sigma_c}{E t_c} = \frac{\sigma_c C^*}{E l_s} \quad (1)$$

where σ_c is the compressive strength, t_c is the time to propagate a crack along entire specimen, and $\dot{\varepsilon}^*$ is the strain rate. This time is equal to the characteristic length divided by the crack propagation velocity, C^*. Assuming that the crack propagation velocity, C^* is equal to 0.2 C_S, where C_S is the shear wave velocity, one obtains: $\dot{\varepsilon}^* \approx 2\times10^3 s^{-1}$ (σ_c= 5 GPa; E= 440 GPa; l_S=7.6 mm; C_S=7,600 m/s). This is slightly above the strain rate used in the Hopkinson bar in the current experiments (400 to 800 s^{-1}) and explains the virtual absence in strain-rate dependence observed.

4. CONFINED EXPERIMENTS (INTERFACE DEFEAT)

SiC-II was used in the impact experiment, which defeated the projectile on the interface (interface defeat). The experiment was carried out by Hauver et al.[5-7]; the experimental details can be found in these sources. The comminuted particle size was around 5 μm, which was similar to the initial grain size. The cross-section of the comminuted zone has an elliptical morphology, and there is a thin, undamaged frontal layer, separating the comminution zone and the impact surface(Fig.3).

This layer contains visible radial cracks, but has no apparent comminution. The initial impact

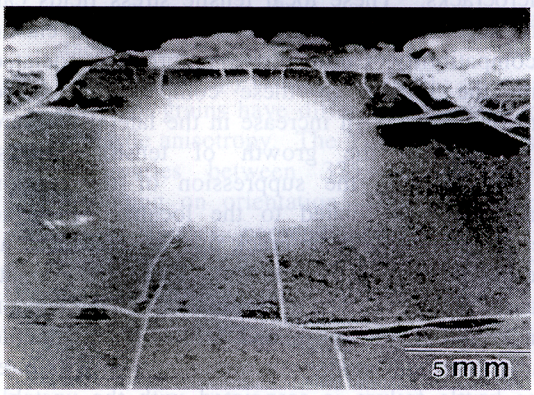

Figure 3. Overview micrograph of recovered SiC

velocity was 1579 m/s. After penetrating through he shock-wave attenuator and the front support, the impact velocity at the ceramic front face was approximately 1482 m/s . At a distance from the interface smaller than the radius of the projectile, a state of uniaxial strain can be assumed, because this region was shielded from the radial release waves. The hydrostatic steady state pressure (P_H) generated by the advancing projectile can be calculated, using the impact velocity (V) and projectile density (ρ_p), through the Bernoulli equation:

$$P_H = \frac{1}{2}\rho_P V^2 \approx 19\ \text{GPa} \qquad (2)$$

At the interface, rod impact also generates a shock pressure, which was attenuated rapidly across the ceramic target. Using the simplest equation of state the pressure on the projectile (P_p), equal to the pressure of the target (P_t), can be estimated, as outlined by Meyers [1]. The interface would undergo a shock pressure as high as 32 Gpa if there were no attenuation; this is an upper estimate for the impact pressure.

Transmission electron microscopy of the regions adjoining the impact of the projectile was carried out by extracting foils parallel to the impact direction (and parallel to the frontal plane of SiC). A grain with profuse dislocations is shown in Figure 4. These dislocations tend to be straight and are aligned along preferred crystallographic directions. The dark field image of Fig. 4 enables the identification of two clear orientations. Thus, dislocations are generated by impact; dislocations and stacking faults were also observed after Hopkinson bar experiments.

Compressive failure of brittle material is different from tensile failure. In compression, microcracks are nucleated at preexisting flaws and local tensile fields are required to propagate the microcracks. These local tensile stress fields can have several origins, and one of the origins is elastic incompatibility. Compressive failure is associated with the growth of these compression-induced tension cracks. An increase in the lateral pressure can suppress the growth of tension cracks. Microscopically, the suppression of the tension cracks can be related to the localized inelastic deformation around the crack tips, as referred to as the plastic zone in Figure 5(a). Horii and Nemat-Nasser [15] developed a formulation for the tension cracks and plastic zones, and defined brittle, ductile and transitional modes for the compressive failure. The brittle failure is associated with the unstable growth of tension cracks; the ductile failure is

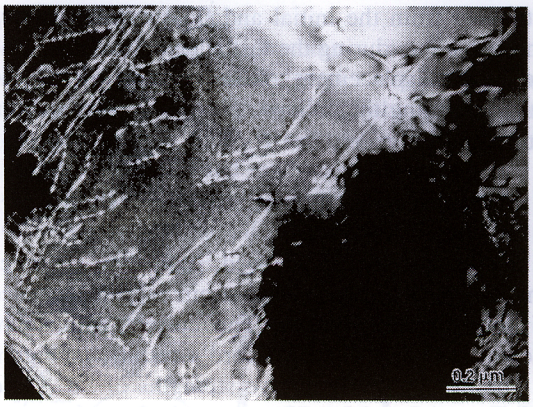

(a)

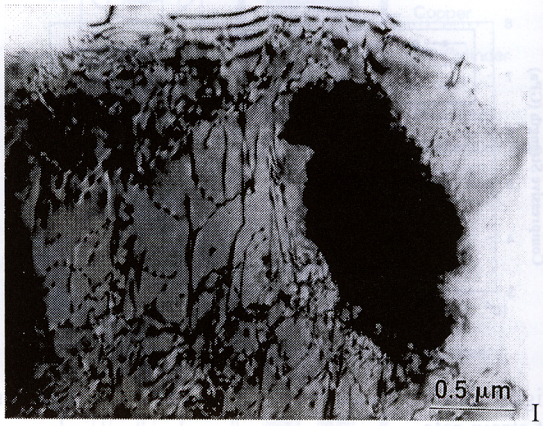

(b)

Figure 4. Dislocations at immediate vicinity (10μm) from impact interface ;(a) dark field; (b) bright field.

dominated by the growth of plastic zones. The transitional mode involves both plastic zones and tension cracks: plastic zones are developed in the early stage, but the final failure is determined by the unstable growth of tension cracks.

The regions of dominance of these three modes are determined by the lateral confinement (σ_{22}/σ_{11}) and a ductility parameter (Δ), as shown in Figure 5(b); the ductility parameter is defined as

$$\Delta = \frac{K_c}{\tau_y \sqrt{\pi c}} \qquad (3)$$

where K_c is the critical stress intensity factor, τ_y is the shear strength, and 2c is the flaw size.

Since the Hugoniot elastic limit is conventionally considered as the maximum stress for elastic response under uniaxial strain, the shear strength can be approximated as half of the

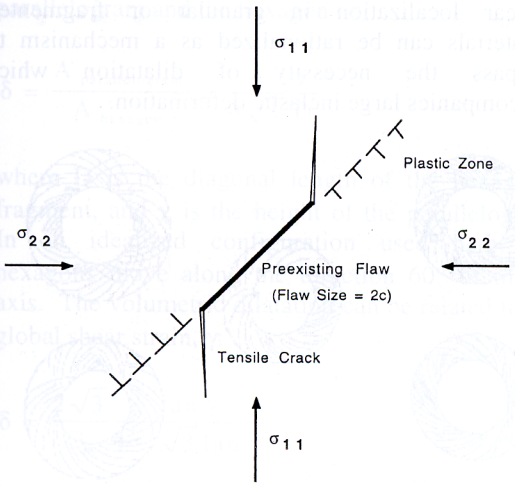

(a)

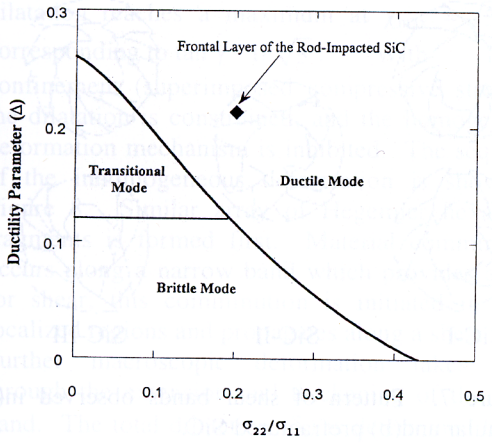

(b)

Figure 5. Compressive failure of brittle materials (adapted from Nemat-Nasser and Hori [16]): (a) plastic zone around the crack tip; (b) brittle-ductle diagram.

Hugoniot elastic limit. Cracks propagate along grain boundaries, so that the flaw size (2c) can be approximated by the grain size. K_c of SiC is 4.1 MPa$\sqrt{m}$, and the ductility parameter can then be estimated: $\Delta = 0.21$.

The Poisson's ratio for SiC is about 0.17, and the lateral confinement can therefore be obtained: $\sigma_{22}/\sigma_{11}= 0.20$. As shown in Figure 5(b), the frontal layer falls into the region for ductile failure mode. In accordance with the model proposed by Horii and Nemat-Nasser [15] suggesting the presence of the plastic zones, the TEM analysis clearly shows the presence of dislocations. The high lateral confinement and its intrinsic high ductility parameter allow the material to deform inelastically; as a result, the frontal layer does not exhibit significant comminution during impact.

There are a number of microstructural mechanisms that have been identified as failure initiation sites in compressive loading; the ones briefly described below are the most likely failure initiation mechanisms for SiC. There is a hierarchy of defects, which varies according to the processing and composition of material. Thus, SiC-I and SiC–II may have a different mix of defects, resulting in differences in their mechanical response. The principal mechanisms are:

a) Flaws. Figure 6(a) shows a flaw that was produced by the debonding along a grain boundary. This is a common occurrence in polycrystalline brittle materials, because the grain boundaries often contain foreign atoms and second phases. Upon compression, there is slippage on the flaw, producing tensile stresses at the extremities and triggering the formation of cracks.

b) Voids and Inclusions (Fig. 6(b)). These are classic failure initiation sites in ceramics. They are almost always present and result from imperfect processing procedures. These defects are often located at the grain boundaries. Tension stresses are generated at the North and South poles of voids.

c) Stress concentration due to dislocation pileups (Fig. 6(c)). Microcracks can be nucleated from piled up dislocations. The dislocations are often stopped and piled up along their slip planes at obstacles, such as grain boundaries. A high shear stress is generated at the leading dislocation of the pile up, and this stress can be relaxed through the nucleation of a microcrack (Zener-Stroh crack).

d) Stress concentration due to twinning and stacking faults (Fig. 6(d)).

e) Elastic anisotropy effect (Fig. 6(e)). Different grains have different stiffnesses, due to elastic anisotropy. The Young's modulus of SiC varies between 375 and 475 Gpa, depending on orientation. This can generate tensile stresses, perpendicular to the loading direction, of 220 MPa, when the external traction is 5 GPa (compressive strength).

These stresses are higher along the grain boundaries and inside the stiffest grains. It should be mentioned that initiation mechanisms a, c, and d produce intergranular microcracks, whereas b and e

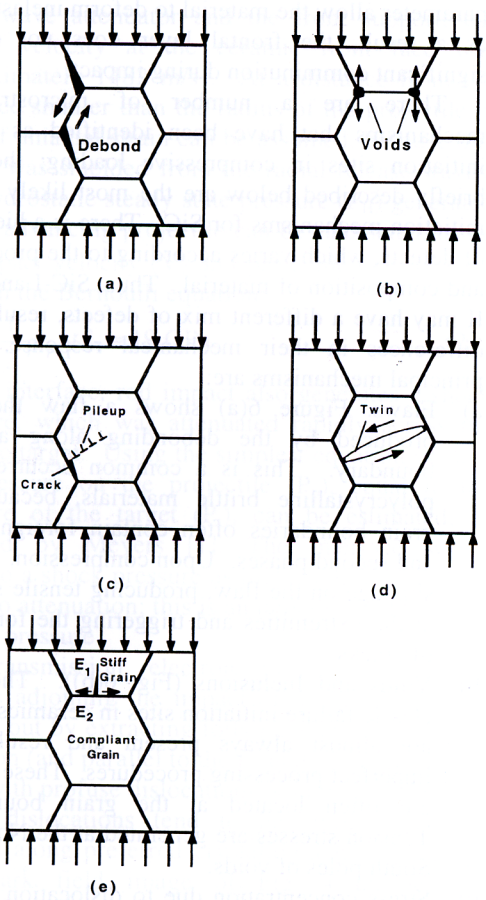

Figure 6. Schematic overview of principal damage initiation mechanisms in SiC: (a) grain boundary debonds; (b) voids and foreign particles, such as inclusions; (c) dislocation pileups, leading to Zener-Stroh cracks; (d) twins and stacking faults; (e) dilatant crack produced by elastic anisotropy($E_1<E_2$).

produce transgranular microcracks.

5. FRAGMENTED AND GRANULAR MATERIAL RESPONSE

Figure 7 shows the pattern of shear bands observed in granular and prefractured SiC. A substantial fraction of the global strain is accommodated by shear deformation within shear localization zones. The flow of ceramics under dynamic loading is much less understood than that of metals, which has been extensively investigated. In granular Al_2O_3, Nesterenko et al.[11] observed shear localization which is due to a softening mechanism not directly attributed to thermal effects. Shear localization in granular or fragmented materials can be rationalized as a mechanism to bypass the necessity of dilatation which accompanies large inelastic deformation.

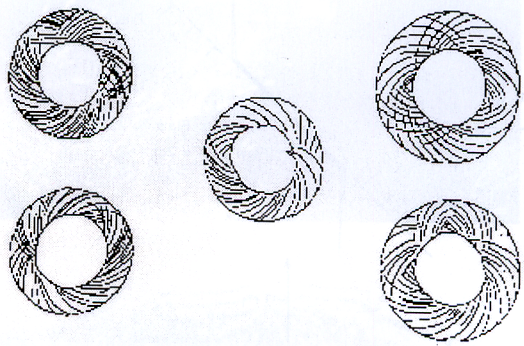

(a)Small(0.4 μm), Medium(3 μm), Large(50 μm)

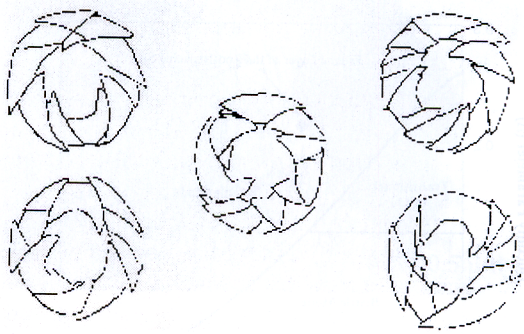

(b)SiC-I SiC-II SiC-III

Figure 7. Pattern of shear bands observed in(a) granular and(b) prefractured SiC.

Under small or no confinement, the deformation of a fragmented ceramic will exhibit dilatation. Curran et al. [18] developed a micromechanical model using two-dimensional square blocks with voids and dislocation arrays. The deformation of fragmented materials is carried out through the sliding of the square blocks. Hegemier [17] proposed a hexagonal network of fragments to represent a fractured ceramic. Hegemier's approach can be used to model dilatation. Upon deformation, the hexagonal fragments move with respect to each other opening crack surfaces (Fig. 8). This are the so-called Hegemier hexagons. These hexagons represent the fragmented material. In order to produce inelastic deformation, the individual hexagons have to slide. The volumetric dilatation (ratio of the void volume to the solid volume) can

be represented by the areal ratio between the dashed parallelogram and the hexagon:

$$\delta = \frac{A_{\text{parallelogram}}}{A_{\text{hexagon}}} = \frac{4}{3\sqrt{3}} \frac{\chi}{D} \qquad (4)$$

where D is the diagonal length of the hexagonal fragment, and χ is the height of the parallelogram. In an idealized configuration used here, the hexagons move along the direction 60° of the x-axis. The volumetric dilatation can be related to the global shear strain, γ:

$$\delta = \frac{2\sqrt{3}}{3} \frac{\tan\gamma}{1 - \sqrt{3}\tan\gamma} \qquad (5)$$

As the deformation continues, the dilatation increases approximately linearly with strain. The dilatation reaches a maximum at $\chi_{max} = \sqrt{3}\, D/4$, corresponding to $\tan\gamma = 1/\sqrt{3}$. With lateral confinement (superimposed compressive stresses), the dilatation is constrained, and the homogeneous deformation mechanism is inhibited. The sequence of the inhomogeneous deformation is shown in Figure 8. Similar array of Hegemier hexagonal fragments is formed first. Material comminution occurs along a narrow band which provides a path for shear; this comminution is initiated in some localized regions and propagates along a shear band. Further macroscopic deformation takes place through the extension and thickening of the shear band. The total dilatation (δ_t) is determined by the dilatation inside the shear band (δ_s):

$$\delta_t = \delta_s \frac{T}{S} \qquad (6)$$

where T is the shear band thickness, and S is the shear band spacing. In this inhomogeneous deformation process, the Hegemier mechanism is applicable inside the concentrated shear bands, and shear localization regions (see detail in Figure 9(b)), with a reduction in scale of the unit hexagons.

Therefore, one can consider a constant dilatation inside the shear band; i.e., $\delta_s = \delta_m = 0.16$. Figures 9(c) and (d) show the evolution of the shear band through its thickening. It propagates and incorporates the surrounding material. The same effects were observed for prefractured and granular Al_2O_3 [11]. One can state that the shear band

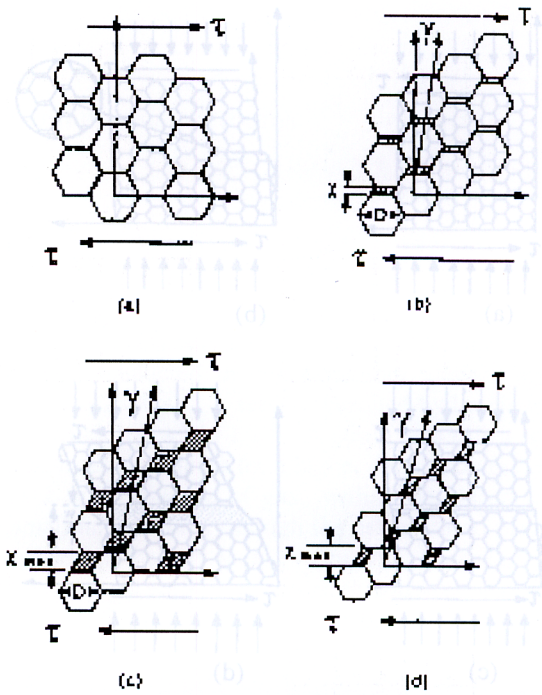

Figure 8. Hegemier hexagons; (a) initial configuration of fragments; (b)sliding with dilatation χ; (c)maximumm dilatation; (d)decrease of dilatation at end of cycle.

spacing is a characteristic scale that is governed by the release of elastic energy stored in the collapsing cylinder. The granular material, with a lower resistance to shear flow has a lower shear-band spacing.

In summary, the shear-band spacing introduces a new scale in fragmented materials: the size of fragmented blocks. The material movement outside the shear localization bands can be considered mainly as the deformation within the fragmented blocks. This deformation is carried out by comminution, through propagating comminution fronts.

In the small particle-sized SiC a unique phenomenon was observed. The particles did not break up in this region, but underwent plastic deformation with the generation of heat. Figure 10 shows the micro-indentation markings that were made on the dense SiC layer in the shear bands.

The material did not crumble; on the contrary, the indentation markings are clear and confirm that the powder is fully bonded inside the shear localization regions. The hardness value obtained is 26 GPa, which compares favorably with a reported hardness of 23 GPa for fully dense SiC. The

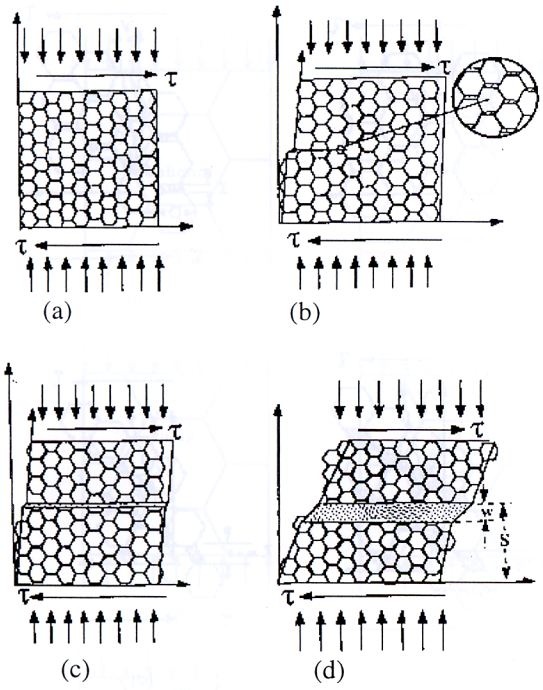

Figure 9. Inhomogeneous deformation under high lateral confinement: (a) formation of hexagonal fragments, (b) initiation of shear band, (c) developed shear band, and (d) propagation of shear-band and thickening.

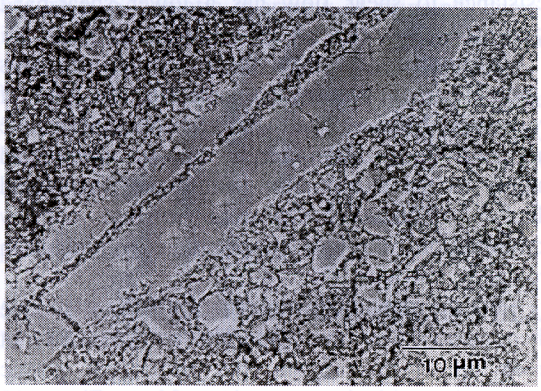

Figure 10. Sintering in shear band of medium powder with large displacement

difference could be due to the small load (10 gf) used in the current experiments. It is thought that the strong bonding between the particles, under the influence of high superimposed pressure, is associated with the combined (and coupled) effects of intense plastic deformation and heating, during the shear localization event. This is indeed surprising and is a novel phenomenon, since conventional sintering requires times that are many orders of magnitude higher. The possibility of accelerated diffusion due to the generation of large dislocation densities in the deforming particles should be considered.

6.CONCLUSIONS

The principal conclusions of this investigation are:

a) The impact velocities characteristic of armor applications generate a substantial amount of dislocations in SiC, yielding a region with profound "microplasticity" effects. Stacking faults and polytype transformations are also produced.

b) Microplasticity may play an important role in the initiation of fracture through micromechanical processes. This was first pointed out by Lankford [12,13] in al and is here by confirmed for silicon carbide.

c) The flow of comminuted material is an essential component of penetration of heavy (confirmed) armor. In light (unconfirmed) armor, the structural bending and disintegration of ceramic plates is more important.

d) It is demonstrated that the flow of granular or fragmented ceramic involves shear localization in a prominent manner. This shear localization is modeled through the Hegemier hexagons. In the granular material, the coarser powder undergoes fragmentation within the shear bands, whereas the finer powder deforms and heats up, reaching temperatures sufficient for sintering inside of the shear bands.

ACKNOWLEDGEMENT

This research was funded by the MURI program (DAAH04-96-1-0376) and by the National Science Foundation Institute for Mechanics and Materials. The invaluable help of Dr. E. Rapacki and Dr. G. Hauver at ARL in providing the rod-impacted specimens and of Mr. J. Isaacs in training and assistance in Hopkinson bar experiments is greatly appreciated. Dr. S. J. Chen (NCEM) provided magnificent help with transmission electron microscopy and the facilities of the National Center for Electron Microscopy were used in this research.

REFERENCES

1. M.A. Meyers, Dynamic Behavior of Materials,

J. Wiley, NY, 1994.
2. J. Shih, V. F. Nesterenko, and M. A. Meyers, J. Appl. Phys., **83** (1998) 4660.
3. J. Shih, M. A. Meyers, and V. F. Nesterenko, Acta Mat.,**46** (1997) 4037.
4. J. Shih, M. A. Meyers, V. F. Nesterenko, and S. J. Chen, Acta Mat.,**48** (2000) 2399.
5. G.E. Hauver, P.H. Netherwood, R.F. Benck, and L.J Kecskes, in "Proceedings of 13th Army Symposium on Solid Mechanics", 1993, p. 23.
6. G.E. Hauver, P.H. Netherwood, R.F. Benck, and L.J. Kecskes, in "Proceedings of 19th Army Science Conference", 1994, p.1.
7. E. J. Rapacki, G. E. Hauver, P.H. Netherwood, and R.Benck, "Ceramics for Armors-A Materials System Perspective", 19th Ann. TARDEC Ground Vehicle Surv. Symp., March, 1996, Monterrey, Ca.
8. M.P. Bondar and V.F. Nesterenko, J. de Physique IV **1**(1991).C3 163
9. V.F. Nesterenko and M.P. Bondar, Dymat J., **1**(1994) 245.
10. V.F. Nesterenko, M.A. Meyers, H.C. Chen, and J.C. LaSalvia, Metall. Mater. Trans., A **26A** (1995) 2511.
11. V. F. Nesterenko, M.A. Meyers, and H.C. Chen, Acta Mat., **44** (1996) 2017.
12. J.Lankford, in "Fracture Mechanics of Ceramics", vol. 5, Plenum Press, New York, 1983, p. 625.
13. J. Lankford, J. Am. Cer. Soc., **64** (1981) C-33.
14. G. Ravichandran and G. Subhash, G., Intl. J. Solids and Structures, **32** (1994) 2627.
15. H. Horii and S. Nemat-Nasser, Phil. Trans. Roy. Soc. Lond., **319** (1986) 337.
16. S. Nemat-Nasser, and M. Hori, "Micromechanics: Overall Properties of Heterogeneous Materials", North-Holland,1993, 180-185.
17. G. Hegemier, UCSD, private communication, 1991.
18. D.R. Curran, L. Seaman, T. Cooper, and D.A. Shockey, Int. J. Impact Eng., **13** (1993) 53.